Plankton networks driving carbon export in the oligotrophic ocean

Lionel Guidi, Samuel Chaffron, Lucie Bittner, Damien Eveillard, Abdelhalim
Larhlimi, Simon Roux, Youssef Darzi, Stéphane Audic, L. Berline, Jennifer R.
Brum, et al.

Title:

Plankton networks driving carbon export in the oligotrophic ocean

Authors: Lionel Guidi[1,2,*], Samuel Chaffron[3,4,5,*], Lucie Bittner[6,7,8,*], Damien Eveillard[9,*], Abdelhalim Larhlimi[9], Simon Roux[10,11], Youssef Darzi[3,4], Stephane Audic[8], Léo Berline[1,12], Jennifer Brum[10,11], Luis Pedro Coelho[13], Julio Cesar Ignacio Espinoza[10], Shruti Malviya[7], Shinichi Sunagawa[13], Céline Dimier[8], Stefanie Kandels-Lewis[13,14], Marc Picheral[1], Julie Poulain[15], Sarah Searson[1,2], *Tara* Oceans coordinators, Lars Stemmann[1], Fabrice Not[8], Pascal Hingamp[16], Sabrina Speich[17], Mick Follows[18], Lee Karp-Boss[19], Emmanuel Boss[19], Hiroyuki Ogata[20], Stephane Pesant[21,22], Jean Weissenbach[15,23,24], Patrick Wincker[15,23,24], Silvia G. Acinas[25], Peer Bork[13,26], Colomban de Vargas[8], Daniele Iudicone[27], Matthew B. Sullivan[10,11], Jeroen Raes[3,4,5], Eric Karsenti[7,14], Chris Bowler[7], Gabriel Gorsky[1]

[*] These authors contributed equally to this work

Affiliations:

[1.] Sorbonne Universités, UPMC Université Paris 06, CNRS, Laboratoire d'oceanographie de Villefranche (LOV), Observatoire Océanologique, Villefranche-sur-Mer, France
[2.] Department of Oceanography, University of Hawaii, Honolulu, Hawaii, USA
[3.] Department of Microbiology and Immunology, Rega Institute, KU Leuven, Herestraat 49, 3000 Leuven, Belgium.
[4.] Center for the Biology of Disease, VIB, Herestraat 49, 3000 Leuven, Belgium.
[5.] Department of Applied Biological Sciences, Vrije Universiteit Brussel, Pleinlaan 2, 1050 Brussels, Belgium.
[6.] Sorbonne Universités, UPMC Univ Paris 06, CNRS, Institut de Biologie Paris-Seine (IBPS), Evolution Paris Seine, F-75005, Paris, France.
[7.] Ecole Normale Supérieure, PSL Research University, Institut de Biologie de l'Ecole Normale Supérieure (IBENS), CNRS UMR 8197, INSERM U1024, 46 rue d'Ulm, F-75005 Paris, France.
[8.] Sorbonne Universités, UPMC Université Paris 06, CNRS, Laboratoire Adaptation et Diversité en Milieu Marin, Station Biologique de Roscoff, Roscoff, France
[9.] LINA UMR 6241, Université de Nantes, EMN, CNRS, 44322 Nantes, France.
[10.] Department of Ecology and Evolutionary Biology, University of Arizona, Tucson, AZ, 85721, USA.
[11.] Current affiliation: Department of Microbiology, The Ohio State University, Columbus OH 43210, USA
[12] Current affiliation: Aix-Marseille Univ., Mediterranean Institute of Oceanography (MIO), 13288, Marseille, Cedex 09, France ; Université du Sud Toulon-Var, MIO, 83957, La Garde cedex, France ; CNRS/INSU, MIO UMR 7294; IRD, MIO UMR235.
[13.] Structural and Computational Biology, European Molecular Biology Laboratory, Meyerhofstr. 1, 69117 Heidelberg, Germany,
[14.] Directors' Research European Molecular Biology Laboratory Meyerhofstr. 1 69117 Heidelberg Germany,
[15.] CEA - Institut de Génomique, GENOSCOPE, 2 rue Gaston Crémieux, 91057 Evry France.
[16.] Aix Marseille Université CNRS IGS UMR 7256 13288 Marseille France
[17.] Department of Geosciences, Laboratoire de Météorologie Dynamique (LMD), Ecole Normale Supérieure, 24 rue Lhomond 75231 Paris Cedex 05 France.
[18.] Dept of Earth, Atmospheric and Planetary Sciences, Massachusetts Institute of Technology, Cambridge, USA.
[19.] School of Marine Sciences, University of Maine, Orono, USA.
[20.] Institute for Chemical Research, Kyoto University, Gokasho, Uji, Kyoto, 611-0011, Japan.
[21.] PANGAEA, Data Publisher for Earth and Environmental Science, University of Bremen, Bremen, Germany.
[22.] MARUM, Center for Marine Environmental Sciences, University of Bremen, Bremen, Germany.
[23.] CNRS, UMR 8030, CP5706, Evry France.
[24.] Université d'Evry, UMR 8030, CP5706, Evry France.
[25.] Department of Marine Biology and Oceanography, Institute of Marine Sciences (ICM)-CSIC Pg. Marítim de la Barceloneta 37-49 Barcelona E08003 Spain.
[26.] Max-Delbrück-Centre for Molecular Medicine, 13092 Berlin, Germany,
[27.] Stazione Zoologica Anton Dohrn, Villa Comunale, 80121, Naples, Italy.

51 **The biological carbon pump is the process by which CO_2 is transformed to organic**

52 **carbon *via* photosynthesis, exported through sinking particles, and finally sequestered**

53 **in the deep ocean or sediment. While the intensity of the pump correlates with plankton**

54 **community composition, the underlying ecosystem structure and interactions driving**

55 **the process remain largely uncharacterised. Here we use environmental and**

56 **metagenomic data gathered during the *Tara* Oceans expedition to improve our**

57 **understanding of carbon export in the oligotrophic ocean. We show that specific**

58 **euphotic plankton communities correlate with carbon export and highlight unexpected**

59 **and overlooked taxa such as Radiolaria, alveolate parasites, as well as *Synechococcus***

60 **and their phages, as lineages most strongly associated with carbon export in the**

61 **subtropical, nutrient-depleted, oligotrophic ocean. Additionally, we show that the**

62 **relative abundance of just a few bacterial and viral genes can predict most of the**

63 **variability in carbon export in these regions.**

64 Marine planktonic photosynthetic organisms are responsible for approximately fifty percent

65 of Earth's primary production and they fuel the global ocean biological carbon pump[1]. The

66 intensity of the pump is correlated to plankton community composition[2,3], and controlled by

67 the relative rates of primary production and carbon remineralisation[4]. About 10% of this

68 newly produced organic carbon in the surface ocean is exported through gravitational

69 sinking of particles. Finally, after multiple transformations, only a fraction of the exported

70 material will reach the deep ocean where it is sequestered over thousand-year timescales of

71 the ocean's overturning circulation[5].

72 Like most biological systems, marine ecosystems in the sunlit upper layer of the ocean

73 (denoted the euphotic zone) are complex[6,7], characterised by a wide range of biotic and

74 abiotic interactions[8-10] and in constant balance between carbon production, transfer to higher

75   trophic levels, remineralisation, and export to the deep layers[11]. The marine ecosystem

76   structure and its taxonomic and functional composition likely evolved to comply with this

77   loss of energy by modifying organism turnover times and by the establishment of complex

78   feedbacks between them[6] and the substrates they can exploit for metabolism[12]. Decades of

79   groundbreaking research have focused on identifying independently the key players involved

80   in the biological carbon pump. Among autotrophs, diatoms are commonly attributed to being

81   important in carbon flux because of their large size and fast sinking rates[13-15] while small

82   autotrophic picoplankton may contribute directly as a result of subduction of surface water

83   resulting from sub-mesoscale dynamic features[16] or indirectly by aggregating with larger

84   settling particles or through their consumption by organisms at higher trophic levels[17].

85   Among heterotrophs, zooplankton such as copepods impact carbon flux *via* production of

86   fast-sinking fecal pellets while migrating hundreds of meters in the water-column[18,19]. These

87   observations, focusing on just a few components of the marine ecosystem, highlight that

88   carbon export results from multiple biotic interactions and that a better understanding of the

89   mechanisms involved in its regulation will likely require an analysis of the entire planktonic

90   ecosystem.

91   Advanced sequencing technologies now offer the opportunity to simultaneously survey

92   whole planktonic communities and associated molecular functions in unprecedented detail.

93   Such a holistic approach may allow the identification of community- or gene-based

94   biomarkers that could be used to monitor and predict ecosystem functions, e.g., related to the

95   biogeochemistry of the ocean[20-22]. Here, we leverage global-scale ocean genomics

96   datasets[10,23-25] and associated environmental data to assess the coupling between ecosystem

97   structure, functional repertoire, and the carbon export component of the biological carbon

98   pump.

Carbon export and plankton community composition

The *Tara* Oceans global circumnavigation crossed diverse ocean ecosystems and sampled plankton at an unprecedented scale[20,26] (see Methods). Hydrographic data were measured *in situ* or in seawater samples at all stations, as well as nutrients, oxygen and photosynthetic pigments (see Methods). Net Primary Production (NPP) was derived from satellite measurements (see Methods). In addition, particle size distributions (100 μm to a few mm) and concentrations were measured using an Underwater Vision Profiler (UVP) from which carbon export, corresponding to the carbon flux (Fig. 1) at 150 m, was calculated to range from 0.014 to 18.3 mg.m^{-2}.d^{-1} using previously validated methods (see Methods). The approach allowed us to assemble the largest homogeneous carbon flux dataset during a single expedition, corresponding to more than 600 profiles over 150 stations. This dataset is of similar magnitude to the body of historical data available in the literature that includes the 134 deep sediment trap-based carbon flux time-series[27] from the JGOFS program and the 419 thorium-derived particulate organic carbon (POC) export measurements[28].

From 68 globally distributed sites, a total of 7.2 Tb of metagenomics data, representing *circa* 40 million non-redundant genes, around 35,000 Operational Taxonomic Units (OTUs) of prokaryotes (Bacteria and Archaea) and numerous mainly uncharacterized viruses and picoeukaryotes, have been described recently[23,25]. In addition, a set of 2.3 million eukaryotic 18S rDNA ribotypes was generated from a subset of 47 sampling sites corresponding to approximately 130,000 OTUs[24]. Finally, 5,476 viral "populations" were identified at 43 sites from viral metagenomic contigs, only 39 (<0.1%) of which had been previously observed[25] (see Methods). These genomics data combined across all domains of life together with carbon flux estimates and other environmental parameters were used to explore the relationships between marine biogeochemistry and euphotic plankton communities (see

123 Methods) in the oligotrophic open ocean. Our study did not include high latitude areas due to

124 the current lack of available molecular data.

125 Using a method for regression-based modeling of high dimensional data in biology

126 (specifically a sparse Partial Least Square analysis - sPLS[29], Extended data Fig. 1), we

127 detected several plankton lineages for which relative sequence abundance correlated with

128 carbon export and other environmental parameters, most notably with NPP, as expected (Fig.

129 2 and see Supplementary Information SI1). These included diatoms, dinoflagellates and

130 metazoa (zooplankton), lineages classically identified as key contributors to carbon export.

131 **Plankton community networks associated with carbon export**

132 While the analysis presented in Fig. 2 supports previous findings about key organisms

133 involved in carbon export from the euphotic zone[14,15,17-19], it is not able to capture how the

134 intrinsic structure of the planktonic community relates to this biogeochemical process.

135 Conversely, although other recent holistic approaches[10,30,31] used species co-occurrence

136 networks to reveal potential biotic interactions, they do not provide a robust description of

137 sub-communities driven by abiotic interactions. To overcome these issues, we applied a

138 systems biology approach known as Weighted Gene Correlation Network Analysis

139 (WGCNA[32,33]) to detect significant associations between the *Tara* Oceans genomics data and

140 carbon export. This method delineates communities in the euphotic zone that are the most

141 associated with carbon export rather than predicting organisms associated with sinking

142 particles.

143 In brief, the WGCNA approach builds a network in which nodes are features (in this case

144 plankton lineages or gene functions) and links are evaluated by the robustness of co-

145 occurrence scores. WGCNA then clusters the network into modules (hereafter denoted

146 subnetworks) that can be examined to find strong and significant subnetwork-trait

147   relationships. We then filtered each subnetwork using a Partial Least Square (PLS) analysis

148   that emphasizes key nodes (based on the Variable Importance in Projection (VIP) scores; see

149   Methods and Extended data Fig. 1). These particular nodes are mandatory to summarize a

150   subnetwork (or community) related to carbon export. In particular, they are of interest for

151   evaluating (i) subnetwork robustness and (ii) predictive power for a given trait (see Methods

152   and Extended data Fig. 1).

153   We applied WGCNA to the relative abundance tables of eukaryotic, prokaryotic and viral

154   lineages[23-25] and identified unique subnetworks significantly associated with carbon export

155   within each dataset (see Methods and Supplementary Information SI1, SI2, SI3). The

156   eukaryotic subnetwork (subnetwork-trait relationship to carbon export, Pearson cor. = 0.81, p

157   = $5e^{-15}$) contained 49 lineages (Extended data Fig. 2a and Supplementary Information SI2)

158   among which twenty percent represented photosynthetic organisms (Fig. 3a and

159   Supplementary Information SI2). Surprisingly, this small subnetwork's structure correlates

160   very strongly to carbon export (Pearson cor. = 0.87, p = $5e^{-16}$, Extended data Fig. 2d) and it

161   predicts as much as 69% (Leave-One-Out Cross-Validated (LOOCV), R^2 = 0.69) of the

162   variability in carbon export (Extended data Fig. 3a). Only ~6% of the subnetwork nodes

163   correspond to diatoms and they show lower VIP scores than dinoflagellates (Supplementary

164   Information SI2). This is likely because our samples are not from silicate replete conditions

165   where diatoms were blooming (see Methods). Furthermore, our analysis did not incorporate

166   data from high latitudes, where diatoms are known to be particularly important for carbon

167   export, so this result suggests that dinoflagellates have a heretofore unrecognized role in

168   carbon export processes in subtropical oligotrophic 'type' ecosystems, one of the largest

169   biome on Earth. More precisely four of the five highest VIP scoring eukaryotic lineages that

170   correlated with carbon flux were heterotrophs such as Metazoa (copepods), non-

171   photosynthetic Dinophyceae, and Rhizaria (Fig. 3a and Supplementary Information SI2).

172   These results corroborate recent metagenomics analysis of microbial communities from

173   sediment traps in the oligotrophic North Pacific subtropical gyre[34]. Consistently, *in situ*

174   imaging surveys have revealed Rhizarian lineages, made up of large fragile organisms such

175   as the Collodaria, to represent an until now under-appreciated component of global plankton

176   biomass[35], which here also appear to be of relevance for carbon export. Another 14% of

177   lineages from the subnetwork correspond to parasitic organisms, a largely under-explored

178   component of planktonic ecosystems.

179   The prokaryotic subnetwork that associated most significantly with carbon export

180   (subnetwork-trait relationship to carbon export, Pearson cor. = 0.32, $p = 9e^{-03}$) contained 109

181   OTUs (Extended data Fig. 2b and Supplementary Information SI3), its structure correlated

182   well to carbon export (Pearson cor. = 0.47, $p = 5e^{-06}$, Extended data Fig. 2e) and it could

183   predict as much as 60% of the carbon export (LOOCV, $R^2 = 0.60$) (Extended data Fig. 3b).

184   By far the highest VIP score within this community was assigned to *Synechococcus*,

185   followed by *Cobetia*, *Pseudoalteromonas* and *Idiomarina,* as well as *Vibrio* and *Arcobacter*

186   (Fig. 3b and Supplementary Information SI3). Noteworthy, *Prochlorococcus* genera and

187   SAR11 clade fall out of this community, while the significance of *Synechococcus* for carbon

188   export could be validated using absolute cell counts estimated by flow cytometry (Pearson

189   cor. = 0.64, p = $4e^{-10}$, Extended data Fig. 4b). Moreover, *Prochlorococcus* cell counts did not

190   correlate with carbon export (Pearson cor. = -0.13, $p = 0.27$, Extended data Fig. 4a) whereas

191   the *Synechococcus* to *Prochlorococcus* cell count ratio correlated positively and significantly

192   (Pearson cor. = 0.54, $p = 4e^{-07}$, Extended data Fig. 4c), suggesting the relevance of

193   *Synechococcus*,   rather   than   *Prochlorococcus*,   to   carbon   export.   Interestingly,

194   *Pseudoalteromonas*, *Idiomarina*, *Vibrio* and *Arcobacter* (of which several species are known

195   to be associated with eukaryotes[36]) have also been observed in live and poisoned sediment

196   traps[34] and these genera display very high VIP scores in our subnetwork associated with

197   carbon export. Additional genera reported as being enriched in poisoned traps (also known

198   as being associated with eukaryotes) include *Enterovibrio* and *Campylobacter*, and are

199   present as well in our carbon export subnetwork.

200   Interestingly, the viral subnetwork (*n*=277) most related to carbon export (Pearson cor. =

201   0.93, *p* = 2e^{-15}, Extended data Fig. 2c) contained particularly high VIP scores for two

202   *Synechococcus* phages (Fig. 3c and Supplementary Information SI4), which represented a

203   16-fold enrichment (Fisher's exact test *p* = 6.4e^{-09}). Its structure also correlated with carbon

204   export (Pearson cor. = 0.88, *p* = 6e^{-93}, Extended data Fig. 2f) and it could predict up to 89%

205   of the variability of carbon export (LOOCV, $R^2 = 0.89$) (Extended data Fig. 3c). The

206   significance of these convergent results is reinforced by the fact that sequences from these

207   datasets are derived from organisms collected on independent size filters (see Methods), and

208   further implicates the importance of top-down processes in carbon export.

209   With the aim of integrating eukaryotic, prokaryotic, and viral carbon export communities, we

210   synthesized their respective subnetworks using, as a backbone, a single global co-occurrence

211   network established previously[10]. The resulting network focused on key lineages and their

212   predicted co-occurrences (Fig. 4). Lineages with high VIP values (such as *Synechococcus*)

213   are revealed here as hubs of the co-occurrence network[10], illustrating the potentially strategic

214   key roles within the integrated network of lineages under-appreciated by conventional

215   methods to study carbon export in the ocean. Associations between the hub lineages are

216   mostly mutually exclusive which may explain the relatively weak correlation of some of

217   these lineages with carbon export when using standard correlation analyses as shown in Fig.

218   2.

219   **Gene functions associated with carbon export**

220   Given the potential importance of prokaryotic processes influencing the biological carbon

221 pump[22], we used the same analytical approaches to examine the prokaryotic genomic

222 functions associated with carbon export in the annotated Ocean Microbial Reference Gene

223 Catalogue from *Tara* Oceans[23]. We built a global co-occurrence network for functions (i.e.,

224 Orthologous Groups of genes or OGs) from the euphotic zone and identified two

225 subnetworks of functions that are significantly associated with carbon export (Fig. 5a,

226 Extended data Fig. 5a, light and dark green subnetworks; FNET1 and FNET2, respectively,

227 and Extended data Fig. 5c).

228 The majority of functions in FNET1 and FNET2 correlate well with carbon export (FNET1:

229 mean Pearson cor. = 0.45, s.d. 0.09 and FNET2: mean Pearson cor. = 0.34, s.d. 0.10).

230 Interestingly, FNET2 functions (n=220) encode mostly (83%) core functions (i.e., functions

231 observed in all euphotic samples, see Methods) while the majority of FNET1 functions

232 (n=441) are non-core (85%) (see Supplementary Information SI5, SI6), highlighting both

233 essential and adaptive ecological functions associated with carbon export. Top VIP scoring

234 functions in the FNET1 subnetwork are membrane proteins such as ABC-type sugar

235 transporters (Fig. 5a). This subnetwork also contains many functions specific to the

236 *Synechococcus* accessory photosynthetic apparatus (e.g., relating to phycobilisomes,

237 phycocyanin and phycoerythrin; see Supplementary Information SI5), which is consistent

238 with the major role of this genus for carbon export inferred from the prokaryotic subnetwork

239 (Fig. 3b). In addition, functions related to carbohydrates, inorganic ion transport and

240 metabolism, as well as transcription, are also well represented (Fig. 5b), suggesting overall a

241 subnetwork of functions dedicated to photosynthesis and growth.

242 The FNET2 subnetwork contains several functions encoded by genes taxonomically

243 assigned to *Candidatus pelagibacter* and *Prochlorococcus*, known as occupying similar

244 oceanic regions as *Synechococcus*, but overall most of its relative abundance (74%) is

245 taxonomically unclassified (Extended data Fig. 6). Top VIP scoring functions in FNET2 are

246 also membrane proteins and ABC-type sugar transporters, as well as functions involved in

247 carbohydrate breakdown such as a chitinase (Fig. 5a). These features highlight the potential

248 roles of bacteria in the formation and degradation of marine aggregates[37]. Strikingly, 77%

249 and 58%, of OGs with a VIP score > 1 in FNET1 and FNET2, respectively, are functionally

250 uncharacterized[38,39] (Fig. 5b), pointing to the strong need for future molecular work to

251 explore these functions (see Supplementary Information SI5, SI6).

252 The relevance of the identified bacterial functions to predict carbon export was also

253 confirmed by PLS regression (Extended data Fig. 6b and 6c). As proposed for plankton

254 communities, the functional subnetworks predict 41% and 48% of carbon export variability

255 (LOOCV, $R^2 = 0.41$ and 0.48 for FNET1 and FNET2, respectively) with a minimal number

256 of functions (Fig. 5b, 123 and 54 functions with a VIP score > 1 for FNET1 and FNET2,

257 respectively). Finally, higher predictive power was obtained using subnetworks of viral

258 protein clusters (Extended data Fig. 5b, 5d and 7a), predicting 55% and 89% of carbon

259 export variability (LOOCV $R^2 = 0.55$ and 0.89 for VNET1 and VNET2, respectively;

260 Extended data Fig. 7b, Supplementary Information, SI7, SI8), suggesting again the key role,

261 of not only bacteria, but also their phages in biological processes sustaining carbon export at

262 a global level.

263 **Discussion**

264 In this report we have revealed the potential contribution of under-appreciated components

265 of plankton communities, as well as confirmed the importance of prokaryotes and viruses, in

266 the carbon export component of the biological carbon pump in the nutrient-depleted

267 oligotrophic ocean. Carbon export was estimated from particle size distribution at 150 m

268 measured with the UVP, and we assumed similar particle composition across all size classes.

269   Furthermore, because of instrument and method limitations, particles smaller than 250 μm

270   were not used for these estimations (see Methods). These export estimates evaluate how

271   much carbon leaves the euphotic zone, but they are not necessarily related to sequestration,

272   which occurs deeper in the water column and over longer timescales. Overall, the use of the

273   UVP was the only realistic method to evaluate carbon flux over the 3 years expedition

274   because deployment of sediment traps at all stations would have been impossible. While our

275   findings are consistent with the numerous previous studies that have highlighted the central

276   role of copepods and diatoms in the biological carbon pump[14,15,17-19], they place them in an

277   ecosystem context and generate hypotheses as to the processes that determine the intensity of

278   export, such as parasitism and predation. For example, while viruses are commonly assumed

279   to lyse cells and maintain fixed organic carbon in surface waters, thereby reducing the

280   intensity of the biological carbon pump[40], there are hints that viral lysis may increase carbon

281   export through the production of colloidal particles and aggregate formation[41]. Our current

282   study suggests that these latter roles may be more ubiquitous than currently appreciated. The

283   importance of aggregation and cell stickiness as inferred from gene network analysis, should

284   be further explored mechanistically to investigate the biological significance of these

285   findings.

286   The future evolution of the oceanic carbon sink remains uncertain because of poorly

287   constrained processes, particularly those associated with the biological pump. With current

288   trends in climate change, the size and biodiversity of phytoplankton are predicted to decrease

289   globally[42,43]. Furthermore, in spite of the potential importance of viruses revealed in this

290   study, they have largely been ignored because of limitations in sampling technologies.

291   Consequently, as oligotrophic gyres expand and global mean NPP decreases[44], the field is

292   currently unable to predict the consequences for carbon export from the ocean's euphotic

293   zone. By pinpointing key species that appear to be strongly associated with carbon export in

294   these areas, as well as their co-occurences within plankton communities and key microbial

295   functions, the integrated datasets combined with advanced computational techniques used in

296   this study could provide a framework to address this critical bottleneck.

297   One of the grand challenges in the life sciences is to link genes to ecosystems[45], based on the

298   posit that genes can have predictable ecological footprints at community and ecosystem

299   levels[46-48]. The extensive data sets from *Tara* Oceans have allowed us to predict as much as

300   89% of the variability in carbon export from the oligotrophic surface ocean with just a small

301   number of genes, largely with unknown functions, encoded by prokaryotes and viruses.

302   These findings can be used as a basis to include biological complexity and guide

303   experimental work designed to inform modeling of the global carbon cycle and to understand

304   how it influences and is influenced by changes in climate. Such statistical analyses scaling

305   from gene-to-ecosystems may open the way to the development of a new conceptual and

306   methodological framework to better understand the mechanisms underpinning key ecological

307   processes.

References and Notes

1. Field, C. B., Behrenfeld, M. J., Randerson, J. T. & Falkowski, P. Primary production of the biosphere: Integrating terrestrial and oceanic components. *Science* **281**, 237-240, doi:10.1126/Science.281.5374.237 (1998).

2. Boyd, P. W. & Newton, P. Evidence of the potential Influence of planktonic community structure on the interannual variability of particulate organic-carbon flux. *Deep-Sea Res. I.* **42**, 619-639 (1995).

3. Guidi, L. *et al.* Effects of phytoplankton community on production, size, and export of large aggregates: A world-ocean analysis. *Limnol. Oceanogr.* **54**, 1951-1963 (2009).

4. Kwon, E. Y., Primeau, F. & Sarmiento, J. L. The impact of remineralization depth on the air-sea carbon balance. *Nat Geosci* **2**, 630-635 (2009).

5. IPCC. *Climate Change 2013: The Physical Science Basis. Contribution of Working Group I to the Fifth Assessment Report of the Intergovernmental Panel on Climate Change.* (Cambridge University Press, 2013).

6. Kitano, H. Biological robustness. *Nat Rev Genet* **5**, 826-837, doi:10.1038/Nrg1471 (2004).

7. Suweis, S., Simini, F., Banavar, J. R. & Maritan, A. Emergence of structural and dynamical properties of ecological mutualistic networks. *Nature* **500**, 449-452, doi:10.1038/Nature12438 (2013).

8. Chow, C. E. T., Kim, D. Y., Sachdeva, R., Caron, D. A. & Fuhrman, J. A. Top-down controls on bacterial community structure: microbial network analysis of bacteria, T4-like viruses and protists. *ISME J.* **8**, 816-829, doi:10.1038/Ismej.2013.199 (2014).

9. Fuhrman, J. A. Microbial community structure and its functional implications. *Nature* **459**, 193-199, doi:10.1038/Nature08058 (2009).

10. Lima-Mendez, G. *et al.* Determinants of community structure in the global plankton interactome. *Science* **348**, doi:10.1126/science.1262073 (2015).

11. Giering, S. L. C. *et al.* Reconciliation of the carbon budget in the ocean's twilight zone. *Nature* **507**, 480-483 (2014).

12. Azam, F. Microbial control of oceanic carbon flux: The plot thickens. *Science* **280**, 694-696 (1998).

13. Agusti, S. *et al.* Ubiquitous healthy diatoms in the deep sea confirm deep carbon injection by the biological pump. *Nat Commun* **6**, doi:10.1038/Ncomms8608 (2015).

14. Sancetta, C., Villareal, T. & Falkowski, P. Massive Fluxes of Rhizosolenid Diatoms - a Common Occurrence. *Limnol. Oceanogr.* **36**, 1452-1457 (1991).

15. Scharek, R., Tupas, L. M. & Karl, D. M. Diatom fluxes to the deep sea in the oligotrophic north Pacific gyre at station ALOHA. *Mar. Ecol. Prog. Ser.* **182**, 55-67, doi:10.3354/meps182055 (1999).

16. Omand, M. M. *et al.* Eddy-driven subduction exports particulate organic carbon from the spring bloom. *Science* **348**, 222-225, doi:10.1126/science.1260062 (2015).

17. Richardson, T. L. & Jackson, G. A. Small phytoplankton and carbon export from the surface ocean. *Science* **315**, 838-840 (2007).

18. Steinberg, D. K. *et al.* Bacterial vs. zooplankton control of sinking particle flux in the ocean's twilight zone. *Limnol. Oceanogr.* **53**, 1327-1338 (2008).

19. Turner, J. T. Zooplankton fecal pellets, marine snow, phytodetritus and the ocean's biological pump. *Prog. Oceanogr.* **130**, 205-248, doi:10.1016/j.pocean.2014.08.005 (2015).

20. Karsenti, E. *et al.* A Holistic Approach to Marine Eco-Systems Biology. *Plos Biol.* **9**, doi:10.1371/journal.pbio.1001177 (2011).

21. Strom, S. L. Microbial ecology of ocean biogeochemistry: A community perspective. *Science* **320**, 1043-1045, doi:10.1126/Science.1153527 (2008).

22. Worden, A. Z. *et al.* Rethinking the marine carbon cycle: Factoring in the multifarious lifestyles of microbes. *Science* **347**, 1257594, doi:10.1126/Science.1257594 (2015).

23. Sunagawa, S. *et al.* Structure and function of the global ocean microbiome. *Science* **348**, doi:10.1126/science.1261359 (2015).

24. de Vargas, C. *et al.* Eukaryotic plankton diversity in the sunlit ocean. *Science* **348**, doi:10.1126/science.1261605 (2015).

25. Brum, J. R. *et al.* Patterns and ecological drivers of ocean viral communities. *Science* **348**, doi:10.1126/science.1261498 (2015).

26. Bork, P. *et al.* Tara Oceans studies plankton at PLANETARY SCALE. *Science* **348**, 873-873, doi:10.1126/science.aac5605 (2015).

27. Honjo, S., Manganini, S. J., Krishfield, R. A. & Francois, R. Particulate organic carbon fluxes to the ocean interior and factors controlling the biological pump: A synthesis of global sediment trap programs since 1983. *Prog. Oceanogr.* **76**, 217-285, doi:10.1016/j.pocean.2007.11.003 (2008).

365 28 Henson, S. A., Sanders, R. & Madsen, E. Global patterns in efficiency of particulate organic carbon
366   export and transfer to the deep ocean. *Global. Biogeochem. Cy.* **26**, doi:10.1029/2011GB004099
367   (2012).
368 29 Lê Cao, K. A., Rossouw, D., Robert-Granié, C. & Besse, P. A Sparse PLS for Variable Selection when
369   Integrating Omics Data. *Stat Appl Genet Mol* **7**, doi:10.2202/1544-6115.1390 (2008).
370 30 Chaffron, S., Rehrauer, H., Pernthaler, J. & von Mering, C. A global network of coexisting microbes
371   from   environmental   and   whole-genome   sequence   data.   *Genome   Res.*   **20**,   947-959,
372   doi:10.1101/Gr.104521.109 (2010).
373 31 Faust, K. & Raes, J. Microbial interactions: from networks to models. *Nat. Rev. Microbiol.* **10**, 538-
374   550, doi:10.1038/Nrmicro2832 (2012).
375 32 Aylward, F. O. *et al.* Microbial community transcriptional networks are conserved in three domains at
376   ocean basin scales. *Proceedings of the National Academy of Sciences*, doi:10.1073/pnas.1502883112
377   (2015).
378 33 Langfelder, P. & Horvath, S. WGCNA: an R package for weighted correlation network analysis. *Bmc
379   Bioinformatics* **9** (2008).
380 34 Fontanez, K. M., Eppley, J. M., Samo, T. J., Karl, D. M. & DeLong, E. F. Microbial community
381   structure and function on sinking particles in the North Pacific Subtropical Gyre. *Front Microbiol* **6**,
382   Artn 469, doi:10.3389/Fmicb.2015.00/169 (2015).
383 35 Biard, T. *et al.* *In situ* imaging reveals the biomass of large protists in the global ocean. *Nature*
384   (submitted).
385 36 Thomas, T. *et al.* Analysis of the Pseudoalteromonas tunicata Genome Reveals Properties of a
386   Surface-Associated   Life   Style   in   the   Marine   Environment.   *PLoS   ONE   **3**,
387   doi:10.1371/journal.pone.0003252 (2008).
388 37 Azam, F. & Malfatti, F. Microbial structuring of marine ecosystems. *Nat. Rev. Microbiol.* **5**, 782-791,
389   doi:10.1038/nrmicro1747 (2007).
390 38 Shi, Y. M., Tyson, G. W. & DeLong, E. F. Metatranscriptomics reveals unique microbial small RNAs
391   in the ocean's water column. *Nature* **459**, 266-U154, doi:10.1038/nature08055 (2009).
392 39 Yooseph, S. *et al.* The Sorcerer II Global Ocean Sampling expedition: Expanding the universe of
393   protein families. *Plos Biol.* **5**, 432-466, doi:10.1371/journal.pbio.0050016 (2007).
394 40 Suttle, C. A. Marine viruses - major players in the global ecosystem. *Nat. Rev. Microbiol.* **5**, 801-812,
395   doi:10.1038/Nrmicro1750 (2007).
396 41 Weinbauer,   M.   G.   Ecology   of   prokaryotic   viruses.   *Fems   Microbiol   Rev*   **28**,   127-181,
397   doi:10.1016/j.femsre.2003.08.001 (2004).
398 42 Finkel, Z. V. *et al.* Phytoplankton in a changing world: cell size and elemental stoichiometry. *J.
399   Plankton Res.* **32**, 119-137 (2010).
400 43 Sommer, U. & Lewandowska, A. Climate change and the phytoplankton spring bloom: warming and
401   overwintering zooplankton have similar effects on phytoplankton. *Glob. Change Biol.* **17**, 154-162,
402   doi:10.1111/J.1365-2486.2010.02182.X (2011).
403 44 Behrenfeld, M. J. *et al.* Climate-driven trends in contemporary ocean productivity. *Nature* **444**, 752-
404   755 (2006).
405 45 DeLong, E. F. *et al.* Community genomics among stratified microbial assemblages in the ocean's
406   interior. *Science* **311**, 496-503, doi:10.1126/Science.1120250 (2006).
407 46 Gianoulis, T. A. *et al.* Quantifying environmental adaptation of metabolic pathways in metagenomics.
408   *P. Natl. Acad. Sci. USA* **106**, 1374-1379, doi:10.1073/Pnas.0808022106 (2009).
409 47 Tilman, D. *et al.* The influence of functional diversity and composition on ecosystem processes.
410   *Science* **277**, 1300-1302, doi:10.1126/Science.277.5330.1300 (1997).
411 48 Wymore, A. S. *et al.* Genes to ecosystems: exploring the frontiers of ecology with one of the smallest
412   biological units. *New Phytol* **191**, 19-36, doi:10.1111/J.1469-8137.2011.03730.X (2011).
413

Figure Legends:

Figure 1 | Global view of carbon fluxes along the *Tara* Oceans circumnavigation route. Carbon flux in mg.m^{-2}.d^{-1} estimated from particles size distribution and abundance measured with the Underwater Vision Profiler 5 (UVP5).

Figure 2 | Eukaryotic community associated to carbon export seen using standard methods for regression-based modeling of high dimensional data. Eukaryotic lineages associated to carbon export as revealed by sPLS analysis. Correlations between lineages and environmental parameters are depicted as a clustered heatmap and lineages with a correlation to carbon export higher than 0.2 are highlighted.

Figure 3 | Ecological networks reveal key taxa lineages associated with carbon export at global scale. The relative abundances of taxa in selected subnetworks were used to estimate carbon export and to identify key lineages associated with the process. **a,** The selected eukaryotic subnetwork (*n*=49, see Supplementary Information SI2) can predict carbon export with high accuracy (PLS regression, LOOCV, R^2=0.69, see Extended data Fig. 3a). Lineages with the highest VIP score (dots size is proportional to the VIP score in the scatter plot) in the PLS are depicted as red dots corresponding to three Rhizaria (Collodaria, *Collozoum inerme* and *Sticholonche* sp.), one copepod (*Oithona* sp.), one siphonophore (*Lilyopsis*), three Dinophyceae and one ciliate (*Spirotontonia turbinata*). **b,** The selected prokaryotic subnetwork (*n*=109, see Supplementary Information SI3) can predict carbon export with good accuracy (PLS regression, LOOCV, R^2=0.60, see Extended data Fig. 3b). **c,** The selected viral population subnetwork (*n*=277, see Supplementary Information SI4) can predict carbon export with high accuracy (PLS regression, LOOCV, R^2=0.89, see Extended data Fig. 3c). Two viral populations with a high VIP score (red dots) are predicted as *Synechococcus* phages (see Supplementary Information SI4).

Figure 4 | Plankton community network built from eukaryotic, prokaryotic and viral subnetworks related to carbon export. Major lineages were selected within the three subnetworks (VIP > 1). Co-occurrences between all lineages of interest were extracted from a previously established global co-occurrence network (see methods). Only lineages discussed within the study are pinpointed. The resulting graph is composed of 329 nodes, 467 edges, with a diameter of 7, and average weighted degree of 4.6.

Figure 5 | Bacterial functional networks reveal key functions associated with carbon export at global scale. A bacterial functional network was built based on Orthologous Group/Gene (OG) relative abundances using the WGCNA methodology (see Methods) and correlated to classical oceanographic parameters. **a,** Two functional subnetworks (light and dark green, FNET1 (*n*=220) and FNET2 (*n*=441), respectively) are significantly associated with carbon export (FNET1: Pearson cor. 0.42, p = 4e^{-09} and FNET2: 0.54, p = 7e^{-06}, see Extended data Fig. 5a). The highest VIP score functions from top to bottom correspond to red dots from right to left. **b,** Higher functional categories are depicted for functions with a VIP score >1 (PLS regression, LOOCV, FNET1 R^2=0.41 and FNET2 R^2=0.48, see Extended data Fig. 6) in both functional subnetworks,

Methods

Environmental data collection

From 2009-2013, environmental data (Supplementary Information SI9) were collected across all major oceanic provinces in the context of the *Tara* Oceans expeditions[20]. Sampling stations were selected to represent distinct marine ecosystems at a global scale[49]. Note that Southern Ocean stations were not examined herein because they were ranked as outliers due to their exceptional environmental characteristics and biota[23,24]. Environmental data were obtained from vertical profiles of a sampling package[50,51]. It consisted of conductivity and temperature sensors, chlorophyll and CDOM fluorometers, light transmissometer (Wetlabs C-star 25cm), a backscatter sensor (WetLabs ECO BB), a nitrate sensor (SATLANTIC ISUS) and a Hydroptic Underwater Vision Profiler (UVP; Hydroptics[52]. Nitrate and fluorescence to chlorophyll concentrations as well as salinity were calibrated from water samples collected with Niskin bottle[50]. Net Primary Production (NPP) data were extracted from 8 day composites of the Vertically Generalized Production Model (VGPM[53]) at the week of sampling[54]. Carbon fluxes and carbon export, corresponding to the carbon flux at 150 m, were estimated based on particle concentration and size distributions obtained from the UVP[51] and details are presented below.

From particle size distribution to carbon export estimation

Previous research has shown that the distribution of particle size follows a power law over the μm to the mm size range[3,55,56]. This *Junge*-type distribution translates into the following mathematical equation, whose parameters can be retrieved from UVP images:

$$n(d) = ad^k \qquad \text{(eq. 1)}$$

where d is the particle diameter, and exponent k is defined as the slope of the number spectrum when equation (2) is log transformed. This slope is commonly used as a descriptor of the shape of the aggregate size distribution.

The carbon-based particle size approach relies on the assumption that the total carbon flux of particles (F) corresponds to the flux spectrum integrated over all particle sizes:

$$F = \int_0^\infty n(d).m(d).w(d)dd \qquad \text{(eq. 2)}$$

where $n(d)$ is the particle size spectrum, i.e., equation (1), and $m(d)$ is the mass (here carbon content) of a spherical particle described as:

$$m(d) = \alpha d^3 \qquad \text{(eq. 3)}$$

where $\alpha = \pi\rho/6$, ρ is the average density of the particle, and $w(d)$ is the settling rate calculated using Stokes Law:

$$w(d) = \beta d^2 \qquad \text{(eq. 4)}$$

where $\beta = g(\rho - \rho_0)(18\nu\rho_0)^{-1}$, g is the gravitational acceleration, ρ_0 the fluid density, and ν the kinematic viscosity.

In addition, mass and settling rates of particles, *m(d)* and *w(d)*, respectively, are often described as power law functions of their diameter obtained by fitting observed data, $m(d).w(d) = Ad^B$. The

particles carbon flux can then be estimated using an approximation of Eq. 2 over a finite number (x) of small logarithmic intervals for diameter d spanning from 250 μm to 1.5 mm (particles <250 μm and >1.5 mm are not considered, consistent with the method presented by *Guidi et al., [2008]*[57]) such as

$$F = \sum_{i=1}^{x} n_i A d_i^B \, \Delta \, d_i \qquad \text{(eq. 5)}$$

where A=12.5±3.40 and B=3.81 ± 0.70 have been estimated using a global dataset that compared particle fluxes in sediment traps and particle size distributions from the UVP images.

Genomic data collection

For the sake of consistency between all available datasets from the *Tara* Oceans expeditions, we considered subsets of the data recently published in Science[23-25]. In brief, one sample corresponds to data collected at one depth (surface (SRF) or Deep Cholorophyll Maximum (DCM) determined from the profile of chlorophyll fluorometer) and at one station. To study the eukaryotic community in our current manuscript, we selected stations at which we had environmental data and carbon export estimated at 150 m with the UVP and all size fractions. Consequently a subset of 33 stations (corresponding to 56 samples) has been created compared to the 47 stations analyzed in *de Vargas et al.* [2015]. A similar procedure has been applied to the prokaryotic and viral datasets, reducing the *Sunagawa et al.* [2015] prokaryotic dataset to a subset of 104 samples from 62 stations and the *Brum et al.* [2015] viral dataset into a subset of 37 samples from 22 stations (See Supplementary Information SI10). In addition a detailed table is provided summarizing which samples (depth and station) are available for each domain (Supplementary Information SI11).

Eukaryotic taxa profiling

Photic-zone eukaryotic plankton diversity has been investigated through millions of environmental Illumina reads. Sequences of the 18S ribosomal RNA gene V9 region were obtained by PCR amplification and a stringent quality-check pipeline has been applied to remove potential chimera or rare sequences (details on data cleaning in *de Vargas et al.* [2015][24]). For 47 stations, and if possible at two depths (SRF and DCM), eukaryotic communities were sampled in the *piconano-* (0.8-5 μm), *micro-* (20-180 μm) and *meso*-plankton (180-2000 μm) fractions (a detailed list of these samples is given in Supplementary Information SI12). In the framework of the carbon export study, sequences from all size fractions were pooled in order to get the most accurate and statistically reliable dataset of the eukaryotic community. The 2.3 million eukaryotic ribotypes were assigned to known eukaryotic taxonomic entities by global alignment to a curated database[24]. To get the most accurate vision of the eukaryotic community, sequences showing less than 97% identity with reference sequences were excluded. The final eukaryotic relative abundance matrix used in our analyses included 1,750 lineages (taxonomic assignation has been performed using a last common ancestor methodology, and had thus been performed down to species level when possible) in 56 samples from 33 stations. Pooled abundance (number of V9 sequences) of each lineage has been normalized by the total sum of sequences in each sample.

Prokaryotic taxa profiling

To investigate the prokaryotic lineages, communities were sampled in the pico-plankton. Both filter sizes have been used along the *Tara* Oceans transect: up to station #52, prokaryotic fractions correspond to a 0.22-1.6 μm size fraction, and from station #56, prokaryotic fractions correspond to a

533   0.22-3 μm size fraction. Prokaryotic taxonomic profiling was performed using 16S rRNA gene tags
534   directly identified in Illumina-sequenced metagenomes (mitags) as described in *Logares et al.,*
535   [2014][58]. 16S mitags were mapped to cluster centroids of taxonomically annotated 16S reference
536   sequences from the SILVA database[59] (release 115: SSU Ref NR 99) that had been clustered at 97%
537   sequence identity using USEARCH v6.0.307[60]. 16S mitag counts were normalized by the total reads
538   count in each sample (further details in *Sunagawa et al.* [2015][23]). The photic-zone prokaryotic
539   relative abundance matrix used in our analyses included 3,253,962 mitags corresponding to 1,328
540   genera in 104 samples from 62 stations.
541

Prokaryotic functional profiling

543   For each prokaryotic sample, gene relative abundance profiles were generated by mapping reads to
544   the OM-RGC using the MOCAT pipeline[61]. The relative abundance of each reference gene was
545   calculated as gene length-normalized base counts. And functional abundances were calculated as the
546   sum of the relative abundances of these reference genes, annotated to OG functional groups. In our
547   analyses, we used the subset of the OM-RGC that was annotated to Bacteria or Archaea (24.4 M
548   genes). Using a rarefied (to 33 M inserts) gene count table, an OG was considered to be part of the
549   ocean microbial core if at least one insert from each sample was mapped to a gene annotated to that
550   OG. For further details on the prokaryotic profiling please refer to *Sunagawa et al.* [2015][23]. The final
551   prokaryotic functional relative abundance matrix used in our analyses included 37,832 OGs or
552   functions in 104 samples from 62 stations. Genes from functions of FNET1 and FNET2 subnetworks
553   were taxonomically annotated using a modified dual BLAST-based last common ancestor (2bLCA)
554   approach[62]. We used RAPsearch2[63] rather than BLAST to efficiently process the large data volume
555   and a database of non-redundant protein sequences from UniProt (version: UniRef_2013_07) and
556   eukaryotic transcriptome data not represented in UniRef (see Supplementary Information SI5, SI6,
557   for full annotations).

Enumeration of prokaryotes by flow cytometry

559   For prokaryote enumeration by flow cytometry, three aliquots of 1 ml of seawater (pre-filtered by
560   200-μm mesh) were collected from both SRF and DCM. The samples were fixed immediately using
561   cold 25% glutaraldehyde (final concentration 0.125%), left in the dark for 10 min at room
562   temperature, flash-frozen and kept in liquid nitrogen on board and then stored at -80°C on land. Two
563   subsamples were taken to separate counts of heterotrophic prokaryotes (not shown herein) and
564   phototrophic picoplankton. For heterotrophic prokaryote determination, 400 μl of sample was added
565   to a diluted SYTO-13 (Molecular Probes Inc., Eugene, OR, USA) stock (10:1) at 2.5 μmol l^{-1} final
566   concentration, left for about 10 min in the dark to complete the staining and run in the flow
567   cytometer. We used a FacsCalibur (Becton & Dickinson) flow cytometer equipped with a 15 mW
568   Argon-ion laser (488 nm emission). At least 30,000 events were acquired for each subsample (usually
569   100,000 events). Fluorescent beads (1 μm, Fluoresbrite carboxylate microspheres, Polysciences Inc.,
570   Warrington, PA) were added at a known density as internal standards. The bead standard
571   concentration was determined by epifluorescence microscopy. For phototrophic picoplankton, we
572   used the same procedure as for heterotrophic prokaryote, but without addition of SYTO-13. Data
573   analysis was performed with FlowJo software (Tree Star, Inc.).

Profiling of viral populations

575   In order to associate viruses to carbon export we used viral populations as defined in *Brum et al.*
576   [2015][25] using a set of 43 *Tara* Oceans viromes. Briefly, viral populations were defined as large
577   contigs (>10 predicted genes and >10 kb) identified as most likely originating from bacterial or
578   archaeal viruses. These 6,322 contigs remained and were then clustered into populations if they

579   shared more than 80% of their genes at >95% nucleotide identity. This resulted in 5,477
580   'populations' from the 6,322 contigs, where as many as 12 contigs were included per population. For
581   each population, the longest contig was chosen as the 'seed' representative sequence. The relative
582   abundance of each population was computed by mapping all quality-controlled reads to the set of
583   5,477 non-redundant populations (considering only mapping quality scores greater than 1) with
584   Bowtie2[64] and if more than 75% of the reference sequence was covered by virome reads. The relative
585   abundance of a population in a sample was computed as the number of base pairs recruited to the
586   contig normalized to the total number of base pairs available in the virome and the contig length if
587   more than 75% of the reference sequence was covered by virome reads, and set to 0 otherwise (see
588   *Brum et al.* [2015][25] for further details). The final viral population abundance matrix used in our
589   analyses included 5,291 viral population contigs in 37 samples from 22 stations.

Viral host predictions

591   The longest contig in a population was defined as the seed sequence and considered the best estimate
592   of that population's origin. These seed sequences were used to assess taxonomic affiliation of each
593   viral population. Cases where >50% of the genes were affiliated to a specific reference genome from
594   RefSeq Virus (based on a BLASTp comparison with thresholds of 50 for bit score and 10^{-5} for e-
595   value) with an identity percentage of at least 75% (at the protein sequence level) were considered as
596   confident affiliations to the corresponding reference virus. The viral population host group was then
597   estimated based on these confident affiliations (see Supplementary Information SI13 for host
598   affiliation of viral population contigs associated to carbon export).

Viral protein clusters

600   Viral protein clusters (PCs) correspond to ORFs initially mapped to existing clusters (POV, GOS and
601   phage genomes). The remaining, unmapped ORFs were self-clustered, using cd-hit as described in
602   *Brum et al.* [2015][25]. Only PCs with more than two ORFs were considered bona fide and were used
603   for subsequent analyses. To compute PC relative abundance for statistical analyses, reads were
604   mapped back to predicted ORFs in the contigs dataset using Mosaik as described in *Brum et al.*
605   [2015][25]. Read counts to PCs were normalized by sequencing depth of each virome. Importantly, we
606   restricted our analyses to 4,294 PCs associated to the 277 viral population contigs significantly
607   associated to carbon export in 37 samples from 22 stations.

Sparse Partial Least Squares analysis

609   In order to directly associate eukaryotic lineages to carbon export and other environmental traits (Fig.
610   2), we used sparse Partial Least Square (sPLS[65] as implemented in the R package *mixOmics*[29]. We
611   applied the sPLS in regression mode, which will model a causal relationship between the lineages
612   and the environmental traits, *i.e.* PLS will predict environmental traits (*e.g.* carbon export) from
613   lineage abundances. This approach enabled us to identify high correlations (see Supplementary
614   Information SI1) between certain lineages and carbon export but without taking into account the
615   global structure of the planktonic community.

Co-occurrence network model analysis

617   Weighted correlation network analysis (WGCNA) was performed to delineate feature (lineages, viral
618   populations, PCs or functions) subnetworks based on their relative abundance[66,67]. A signed
619   adjacency measure for each pair of features was calculated by raising the absolute value of their
620   Pearson correlation coefficient to the power of a parameter p. The default value p=6 was used for
621   each global network, except for the Prokaryotic functional network where p had to be lowered to 4 in
622   order to optimize the scale-free topology network fit. Indeed, this power allows the weighted

623 correlation network to show a scale free topology where key nodes are highly connected with others.
624 The obtained adjacency matrix was then used to calculate the topological overlap measure (TOM),
625 which for each pair of features, taking into account their weighted pairwise correlation (direct
626 relationships) and their weighted correlations with other features in the network (indirect
627 relationships). For identifying subnetworks a hierarchical clustering was performed using a distance
628 based on the TOM measure. This resulted in the definition of several subnetworks, each represented
629 by its first principal component.

630 These characteristic components play a key role in weighted correlation network analysis. On the one
631 hand, the closeness of each feature to its cluster, referred to as the subnetwork membership, is
632 measured by correlating its relative abundance with the first principal component of the subnetwork.
633 On the other hand, association between the subnetworks and a given trait is measured by the pairwise
634 Pearson correlation coefficients between the considered environmental trait and their respective
635 principal components. A similar protocol has been performed on the eukaryotic relative abundance
636 matrix, the prokaryotic relative abundance matrix, the prokaryotic functions relative abundance
637 matrix and the viral population and PC relative abundance matrices. All procedures were applied on
638 Hellinger-transformed log-scaled abundances. Noteworthy, the protocol is not sensitive to copy
639 number variation as observed across different eukaryotic species, because the association between
640 two species relies on a correlation score between relative abundance measurements. Computations
641 were carried out using the R package *WGCNA*[33].

642 Given the nature of the eukaryotic dataset (three distinct size fractions), the sampling process may
643 lead to the loss of size fractions. In particular, samples #1, #3, #17, #37, #39, #43, #48, #53, #54, #55,
644 #66 are eventually biases by such a loss (Supplementary Information SI12). A complementary
645 WGCNA analysis was performed with addition of these samples to evaluate the robustness of our
646 protocol to missing size fractions. The composition of the eukaryotic subnetwork built with an
647 extended dataset (*i.e.,* 67 samples from 37 stations for which size fractions were missing in 11
648 samples) was compared to the subnetwork as presented above (*i.e.,* 56 samples from 33 stations).
649 Both subnetworks shown an overlap of 75% of lineage, whereas four of the top five VIP lineages
650 with the extended dataset (see Extended data Fig. 8 for details) can be found in the top six VIP
651 lineages of the above subnetwork (Supplementary Information SI2), emphasizing highly similar
652 results and a small sensitivity to size fraction loss.

653 **Extraction of subnetworks related to carbon export**
654 For each subnetwork (called modules within WGCNA) extracted from each global network, pairwise
655 Pearson correlation coefficients between the subnetwork principal components and the carbon export
656 estimation was computed, as well as corresponding p-values corrected for multiple testing using the
657 Benjamini & Hochberg FDR procedure. The subnetworks showing the highest correlation scores are
658 of interest and were investigated. One subnetwork (49 nodes) was significant within the eukaryotic
659 network; one subnetwork (109 nodes) was significant for the prokaryotic network; one subnetwork
660 (277 nodes) was significant within the virus network; two subnetworks (441 and 220 nodes) were
661 significant within the prokaryotic functional network, and two subnetworks (1,879 and 2,147 nodes)
662 were significant within the viral PCs network.

663 **Partial Least Squares regression**
664 In addition to the network analyses, we asked whether the identified subnetworks can be used as
665 predictors for the carbon export estimations. To answer this question, we used Partial least squares
666 (PLS) regression, which is a dimensionality-reduction method that aims at determining predictor

667 combinations with maximum covariance with the response variable. The identified combinations,
668 called latent variables, are used to predict the response variable. The predictive power of the model is
669 assessed by correlating the predicted vector with the measured values. The significance of the
670 prediction power was evaluated by permuting the data 10,000 times. For each permutation, a PLS
671 model was built to predict the randomized response variable and a Pearson correlation was calculated
672 between the permuted response variable and in Leave-One-Out Cross-Validation (LOOCV) predicted
673 values. The 10,000 random correlations are compared to the performance of the PLS model that were
674 used to predict the true response variable. In addition, the predictors were ranked according to their
675 value importance in projection (VIP)[68]. The VIP measure of a predictor estimates its contribution in
676 the PLS regression. The predictors having high VIP values are assumed important for the PLS
677 prediction of the response variable. The VIP values of the prokaryotic functional subnetworks are
678 provided in Supplementary Information SI5, SI6. For the sake of illustration, only lineages or
679 functions with VIP > 1[68] are discussed and pictured in Figure 4 and 5. Our computations were carried
680 out using the R package pls[69]. All programs are available under GPL Licence.

681 **Subnetwork representations**
682 Nodes of the subnetworks represent either lineages (eukaryotic, prokaryotic or viral) or functions
683 (prokaryotic or viral). Subnetworks related to the carbon export have been represented in two distinct
684 formats. Scatter plots represent each nodes based on their Pearson correlation to the carbon export
685 and their respective node centrality within the subnetwork. The latter has been recomputed using
686 significant Spearman correlations above 0.3 (>0.9 for viral PCs) as edges, this is done for
687 visualization purposes since WGCNA subnetworks (based on the Topology Overlap Measure (TOM)
688 between nodes) are hyper-connected. Size representation of nodes are proportional to the VIP score
689 after PLS. The hiveplots depict the same subnetworks by focusing on two main features: x-axis and
690 y-axis depict nodes of subnetworks ranked by their VIP scores and Pearson correlation to the carbon
691 export, respectively.

References and Notes (Methods)

692

693 49 Pesant, S. *et al.* Open science resources for the discovery and analysis of Tara Oceans data. *Scientific*
694 *Data* **2**, 150023, doi:10.1038/sdata.2015.23 (2015).
695 50 Picheral, M. *et al.* Vertical profiles of environmental parameters measured on discrete water samples
696 collected with Niskin bottles during the Tara Oceans expedition 2009-2013.
697 doi:10.1594/PANGAEA.836319 (2014).
698 51 Picheral, M. *et al.* Vertical profiles of environmental parameters measured from physical, optical and
699 imaging sensors during Tara Oceans expedition 2009-2013. doi:10.1594/PANGAEA.836321 (2014).
700 52 Picheral, M. *et al.* The Underwater Vision Profiler 5: An advanced instrument for high spatial
701 resolution studies of particle size spectra and zooplankton. *Limnol. Oceanogr. Meth.* **8**, 462–473,
702 doi:10:4319/lom.2010.8.462 (2010).
703 53 Behrenfeld, M. J. & Falkowski, P. G. Photosynthetic rates derived from satellite-based chlorophyll
704 concentration. *Limnol. Oceanogr.* **42**, 1-20 (1997).
705 54 Chaffron, S. *et al.* Contextual environmental data of selected samples from the Tara Oceans
706 Expedition (2009-2013). doi:10.1594/PANGAEA.840718 (2014).
707 55 McCave, I. N. Size spectra and aggregation of suspended particles in the deep ocean. *Deep-Sea Res. I.*
708 **31**, 329-352 (1984).
709 56 Sheldon, R. W., Prakash, A. & Sutcliff, W. H. Size distribution of particles in ocean. *Limnol.*
710 *Oceanogr.* **17**, 327-340 (1972).
711 57 Guidi, L. *et al.* Relationship between particle size distribution and flux in the mesopelagic zone. *Deep-*
712 *Sea Res. I.* **55**, 1364-1374, doi:10.1016/j.dsr.2008.05.014 (2008).
713 58 Logares, R. *et al.* Metagenomic 16S rDNA Illumina tags are a powerful alternative to amplicon
714 sequencing to explore diversity and structure of microbial communities. *Environ Microbiol* **16**, 2659-
715 2671, doi:Doi 10.1111/1462-2920.12250 (2014).
716 59 Quast, C. *et al.* The SILVA ribosomal RNA gene database project: improved data processing and web-
717 based tools. *Nucleic Acids Res* **41**, D590-D596, doi:10.1093/Nar/Gks1219 (2013).

718 60   Edgar, R. C. Search and clustering orders of magnitude faster than BLAST. *Bioinformatics* **26**, 2460-
719   2461, doi:10.1093/Bioinformatics/Btq461 (2010).
720 61   Kultima, J. R. *et al.* MOCAT: A Metagenomics Assembly and Gene Prediction Toolkit. *PLoS ONE* **7**,
721   ARTN e47656, doi:10.1371/journal.pone.0047656 (2012).
722 62   Hingamp, P. *et al.* Exploring nucleo-cytoplasmic large DNA viruses in Tara Oceans microbial
723   metagenomes. *ISME J.* **7**, 1678-1695, doi:10.1038/Ismej.2013.59 (2013).
724 63   Zhao, Y. A., Tang, H. X. & Ye, Y. Z. RAPSearch2: a fast and memory-efficient protein similarity
725   search   tool   for   next-generation   sequencing   data.   *Bioinformatics*   **28**,   125-126,
726   doi:10.1093/Bioinformatics/Btr595 (2012).
727 64   Langmead, B. & Salzberg, S. L. Fast gapped-read alignment with Bowtie 2. *Nat Methods* **9**, 357-
728   U354, doi:10.1038/Nmeth.1923 (2012).
729 65   Shen, H. P. & Huang, J. H. Z. Sparse principal component analysis via regularized low rank matrix
730   approximation. *J Multivariate Anal* **99**, 1015-1034, doi:10.1016/J.Jmva.2007.06.007 (2008).
731 66   Langfelder, P. & Horvath, S. Eigengene networks for studying the relationships between co-
732   expression modules. *Bmc Syst Biol* **1**, Artn 54, doi:10.1186/1752-0509-1-54 (2007).
733 67   Li, A. & Horvath, S. Network neighborhood analysis with the multi-node topological overlap measure.
734   *Bioinformatics* **23**, 222-231, doi:10.1093/Bioinformatics/Btl581 (2007).
735 68   Chong, I. G. & Jun, C. H. Performance of some variable selection methods when multicollinearity is
736   present. *Chemometr. Intell. Lab.* **78**, 103-112, doi:10.1016/J.Chemolab.2004.12.011 (2005).
737 69   Mevik, B. H. & Wehrens, R. The pls package: Principal component and partial least squares
738   regression in R. *J Stat Softw* **18**, 1-23 (2007).

739

Acknowledgements

Author Contributions

L.G., S.C., Lu.B. and D.E. designed the study and wrote the paper. C.D., M.P., J.P. and Sa.S. collected *Tara* Oceans samples. S.K-L managed the logistics of the *Tara* Oceans project. L.G. and M.P. analysed oceanographic data. S.C. and Lu.B. analysed taxonomic data. S.C., Lu.B., D.E. and S.R. performed the

769 genomic and statistical analyses. A.L., Y.D., L.G., S.C., Lu.B. and D.E. produced and analysed the networks.
770 E.K., C.B. and G.G. supervised the study. M.S., J.R., E.K., C.B. and G.G. provided constructive comments,
771 revised and edited the manuscript. *Tara* Oceans coordinators provided a creative environment and constructive
772 criticism throughout the study. All authors discussed the results and commented on the manuscript.

Author Information

Extended data legends:

Extended Data Figure 1: Overview of analytical methods used in the manuscript. **a,** Depiction of a standard pairwise analysis that considers a sequence relative abundance matrix for s samples (s x OTUs (Operational Taxonomic Units)) and its corresponding environmental matrix (s x p (parameters)). sPLS results emphasize OTU(s) that are the most correlated to environmental parameters. **b,** Depiction of a graph-based approach. Using only a relative abundance matrix (s x OTUs), WGCNA builds a graph where nodes are OTUs and edges represent significant co-occurrence. Co-occurrence scores between nodes are weights allocated to corresponding edges. These weights are magnified by a power-law function until the graph becomes scale-free. The graph is then decomposed within subnetworks (groups of OTUs) that are analyzed separately. One subnetwork (group of OTUs) is considered of interest when its topology is related to the trait of interest; in the current case carbon export. For each subnetwork (for instance the subnetwork related to carbon export), each OTU is spread within a feature space that plots each OTU based on its membership to the subnetwork (x-axis) and its correlation to the environmental trait of interest (i.e., carbon export). A good regression of all OTUs emphasizes the putative relation of the subnetwork topology and the carbon export trait (*i.e.* the more a given OTU defines the subnetwork topology, the more it is correlated to carbon export). **c,** Depiction of the machine learning (PLS) approach that was applied following subnetwork identification and selection. Greater VIP scores (*i.e.* larger circles) emphasized most important OTUs. VIP refers to Variable Importance in Projection and reflects the relative predictive power of a given OTU. OTUs with VIP score greater than one are considered as important in the predictive model and their selection do not alter the overall predictive power.

Extended Data Figure 2: Domain-specific ecological subnetworks associated to environmental parameters and species subnetwork structures correlate to carbon export. **a,b,c,** Global ecological networks were built for the 3 domains of life using the WGCNA methodology (see methods) and correlated to classical oceanographic parameters as well as carbon export (estimated at 150 m from particles size distribution and abundance). Each domain-specific global network is decomposed into smaller coherent subnetworks (depicted by distinct colours on the y-axis) and their eigen vector is correlated to all environmental parameters. Similar to a correlation at the network scale, this approach directly links subnetworks to environmental parameters (*i.e.* the more the taxa contribute to the subnetwork structure, the more their abundance are correlated to the parameter). The measure allows to identify subnetworks for which the overall structure is related to the carbon export. **a,** A single eukaryotic subnetwork (n=58, N=1'870) is strongly associated to carbon export (Pearson cor. 0.81, p = $5e^{-15}$). **b,** A single prokaryotic subnetwork (n=109, N=1'527) is moderately associated to carbon export (Pearson cor. 0.32, p = $9e^{-03}$). **c,** A single viral subnetwork (n=277, N=5'476) is strongly associated to carbon export (Pearson cor. 0.93, p = $2e^{-15}$). **d,e,f,** The WGCNA approach directly links subnetworks to environmental parameters, *i.e.* the more the features contribute to the subnetwork structure (topology), the more their abundance are correlated to the parameter. This measure allows to identify subnetworks for which the overall structure, summarized as the eigen vector of the subnetwork, is related to the carbon export. **d,** The eukaryotic subnetwork structure correlates to carbon export (Pearson cor. = 0.87, p = $5e^{-16}$). **e,** The prokaryotic subnetwork structure correlates to carbon export (Pearson cor. = 0.47, p = $5e^{-06}$). **f,** The viral population subnetwork structure correlates to carbon export (Pearson cor. = 0.88, p = $6e^{-93}$).

Extended Data Figure 3: Species subnetworks predict carbon export. PLS regression was used to predict carbon export using lineage abundances in selected subnetworks. LOOCV was performed and VIP scores computed for each lineage. **a,** The eukaryotic subnetwork predicts carbon export with a R^2 of 0.69. **b,** The prokaryotic subnetwork predicts carbon export with a R^2 of 0.60. **c,** The viral population subnetwork predicts carbon export with a R^2 of 0.89.

Extended Data Figure 4: *Synechococcus* (rather than *Prochlorococcus*) absolute cell counts correlate well to carbon export. **a,** *Prochlorococcus* cell counts estimated by flow cytometry do not correlate to carbon export (mean carbon flux at 150m, Pearson cor. = -0.13, p = 0.27). **b,** *Synechococcus* cell counts estimated by flow cytometry correlate significantly to carbon export

836 (Pearson cor. = 0.64, p = 4.0^{e-10}). **c,** *Synechococcus / Prochlorococcus* cell counts ratio correlates
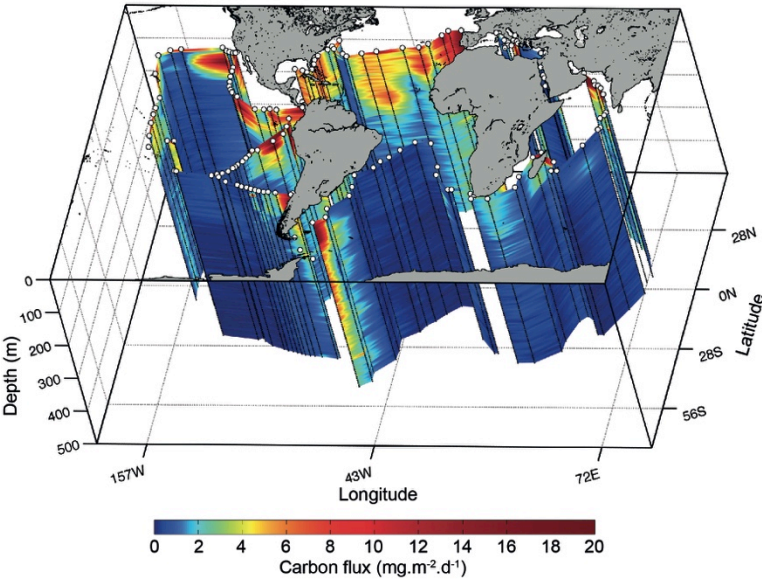837 significantly to carbon export (Pearson cor. = 0.54, p = 4.0^{e-07}).
838
839 **Extended Data Figure 5:** Function and gene subnetworks associated to environmental parameters
840 and their structure correlate to carbon export. **a,b,** Global ecological networks were built for the
841 prokaryotic functions and viral PCs using the WGCNA methodology (see methods) and correlated to
842 classical oceanographic parameters as well as carbon export. Each global network is decomposed into
843 smaller coherent subnetworks (depicted by distinct colours on the y-axis) and their eigen vector is
844 correlated to all environmental parameters. Similar to a correlation at the network scale, this approach
845 directly links subnetworks to environmental parameters (*i.e.* the more the taxa contribute to the
846 subnetwork structure, the more their abundance are correlated to the parameter). The measure allows
847 to identify subnetworks for which the overall structure is related to the carbon export. **a,** Two
848 bacterial functional subnetworks (n=441 and n=220, N=37'832) are associated to carbon export
849 (Pearson cor. 0.54, p = 1^{e-07} and 0.42, p = 1^{e-04}). **b,** Two viral PCs subnetworks (n=1'879 and
850 n=2'147, N=4'678) are strongly associated to carbon export (Pearson cor. 0.75, p = 3^{e-07} and 0.91, p =
851 3^{e-14}). **c,d** The WGCNA approach directly links subnetworks to environmental parameters, *i.e.* the
852 more the features contribute to the subnetwork structure (topology), the more their abundance are
853 correlated to the parameter. This measure allows to identify subnetworks for which the overall
854 structure, summarized as the eigen vector of the subnetwork, is related to the carbon export. **c,** The
855 bacterial function subnetwork structures correlates to carbon export (FNET1 Pearson cor. = 0.68, p =
856 3^{e-61}, and FNET2 Pearson cor. = 0.47, p = 6^{e-13}). **d,** The viral PC subnetwork structures correlates to
857 carbon export (VNET1 Pearson cor. = 0.91, p < 1^{e-200}, and VNET2 Pearson cor. = 0.96, p < 1^{e-200}).
858
859 **Extended Data Figure 6:** Cumulative abnundance of genus-level taxonomic annotations of genes
860 encoding functions from FNET1 and FNET2 subnetworks and Bacterial function subnetworks
861 predict carbon export. **a,** Genes contributing to the relative abundance of FNET1 and FNET2
862 subnetwork functions were taxonomically annotated by homolgy searches against a non-redundant
863 gene reference database using a last common ancestor (LCA) approach (see methods). **b,c,** PLS
864 regression was used to predict carbon export using abundances of functions (OGs) in selected
865 subnetworks. LOOCV was performed and VIP scores computed for each function. **b,** Light green
866 subnetwork (FNET1) functions predict carbon export with a R^2 of 0.41. **c,** Dark green subnetwork
867 (FNET2) functions predict carbon export with a R^2 of 0.48.
868
869 **Extended Data Figure 7:** Viral protein cluster networks reveal potential marker genes for carbon
870 export prediction at global scale. **a,** A viral protein cluster (PC) network was built using abundances
871 of PCs predicted from viral population contigs associated to carbon export (Fig. 3b) using the
872 WGCNA methodology (see methods) and correlated to classical oceanographic parameters. Two
873 viral PC subnetworks (light and dark orange, VNET1 and VNET2, left and right panel respectively)
874 are strongly associated to carbon export (VNET1: Pearson cor. 0.75, p = 3^{e-07} and VNET2: 0.91, p =
875 3^{e-14}, Extended data figure 5b). Size of dots is proportional to the VIP score computed for the PLS
876 regression. **b,** Viral PC subnetworks predict carbon export. PLS regression was used to predict
877 carbon export using abundances of viral protein clusters (PCs) in selected subnetworks. LOOCV was
878 performed and VIP scores computed for each PC. Light orange subnetwork (VNET1, left panel) PCs
879 predict carbon export with a R^2 of 0.55. Dark orange subnetwork (VNET2, right panel) PCs predict
880 carbon export with a R^2 of 0.89.
881
882 **Extended Data Figure 8:** WGCNA and PLS regression analyses for the full Eukaryotic dataset. **a,** A
883 single eukaryotic subnetwork (n=58, is strongly associated to carbon export (Pearson cor. 0.79, p =
884 3^{e-14}). **b,** The eukaryotic subnetwork structure correlates to carbon export (Pearson cor. = 0.94, p = 4^{e-27}).
885 **c,** The eukaryotic subnetwork predicts carbon export with a R^2 of 0.76. **d,** Lineages with the
886 highest VIP score (dots size is proportional to the VIP score in the scatter plot) in the PLS are
887 depicted as red dots corresponding to two rhizarian (Collodaria), one copepod (*Euchaeta*), and three
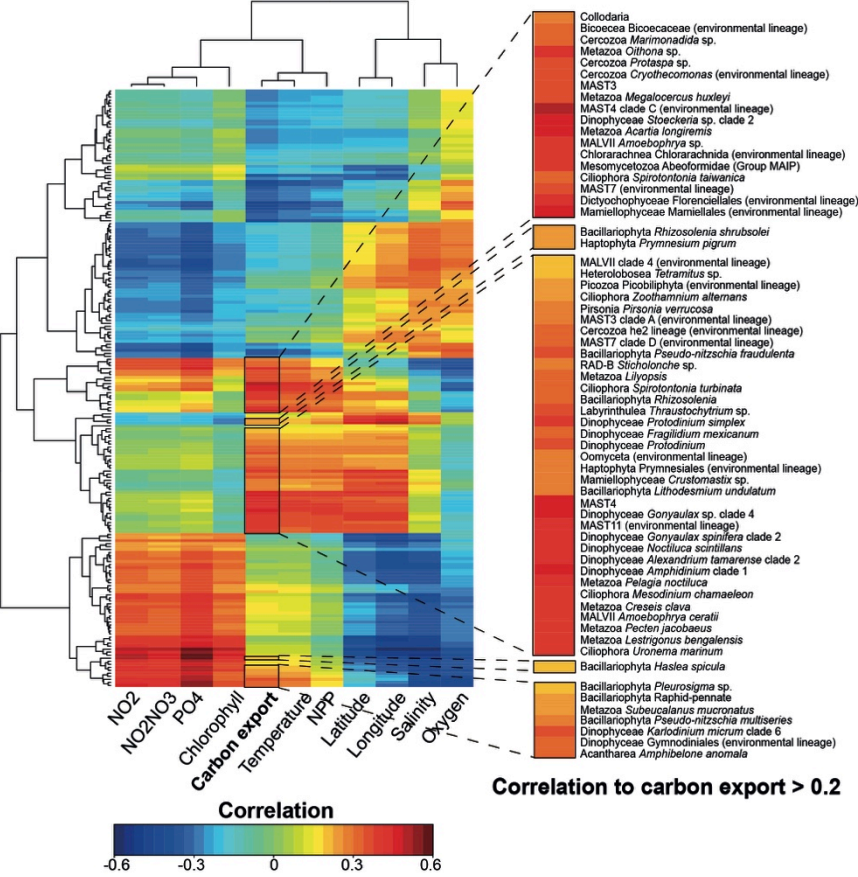888 dinophyceae (*Noctiluca scintillans, Gonyaulax polygramma* and *Gonyaulax sp. (clade 4)*).
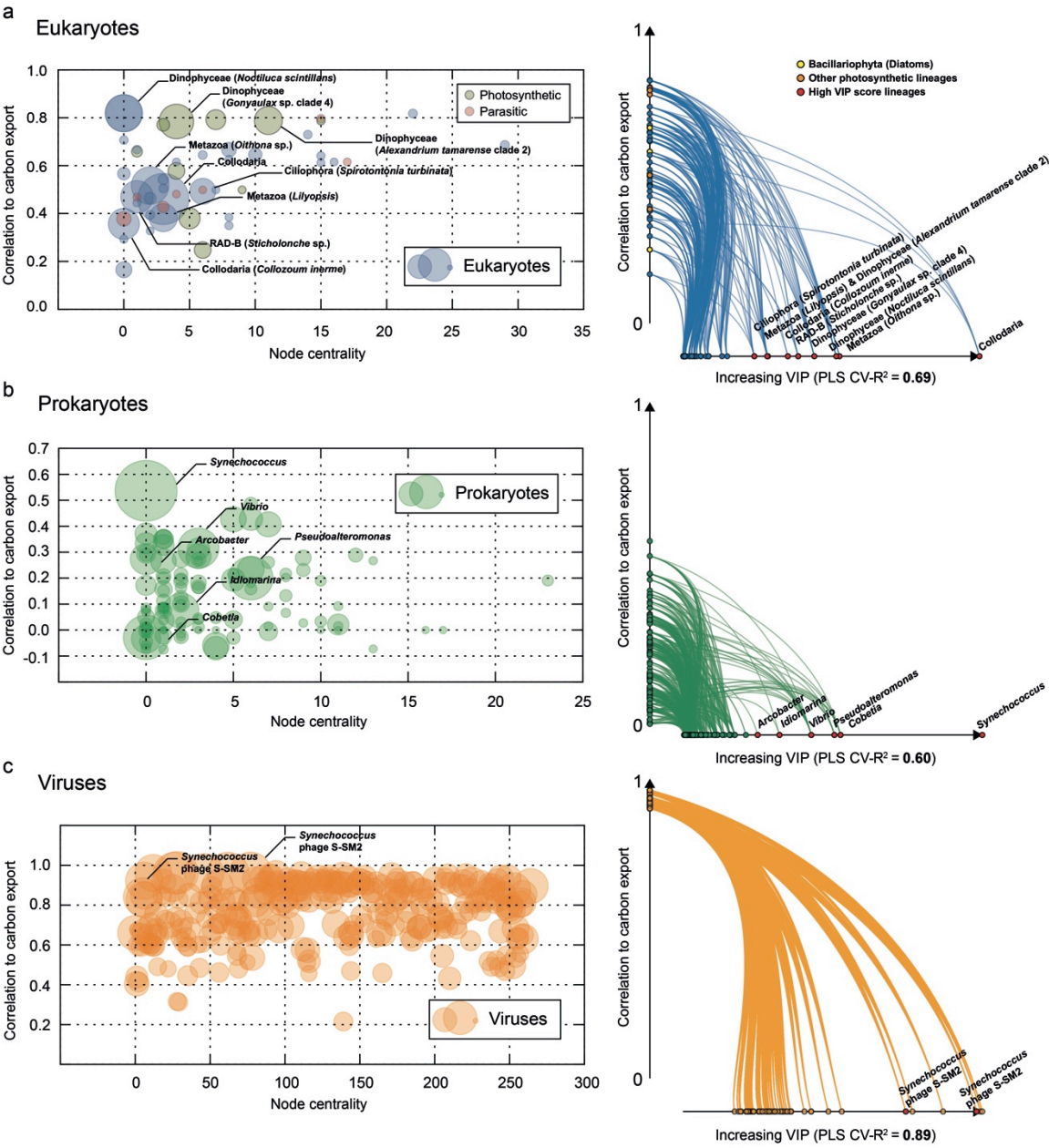
889

890

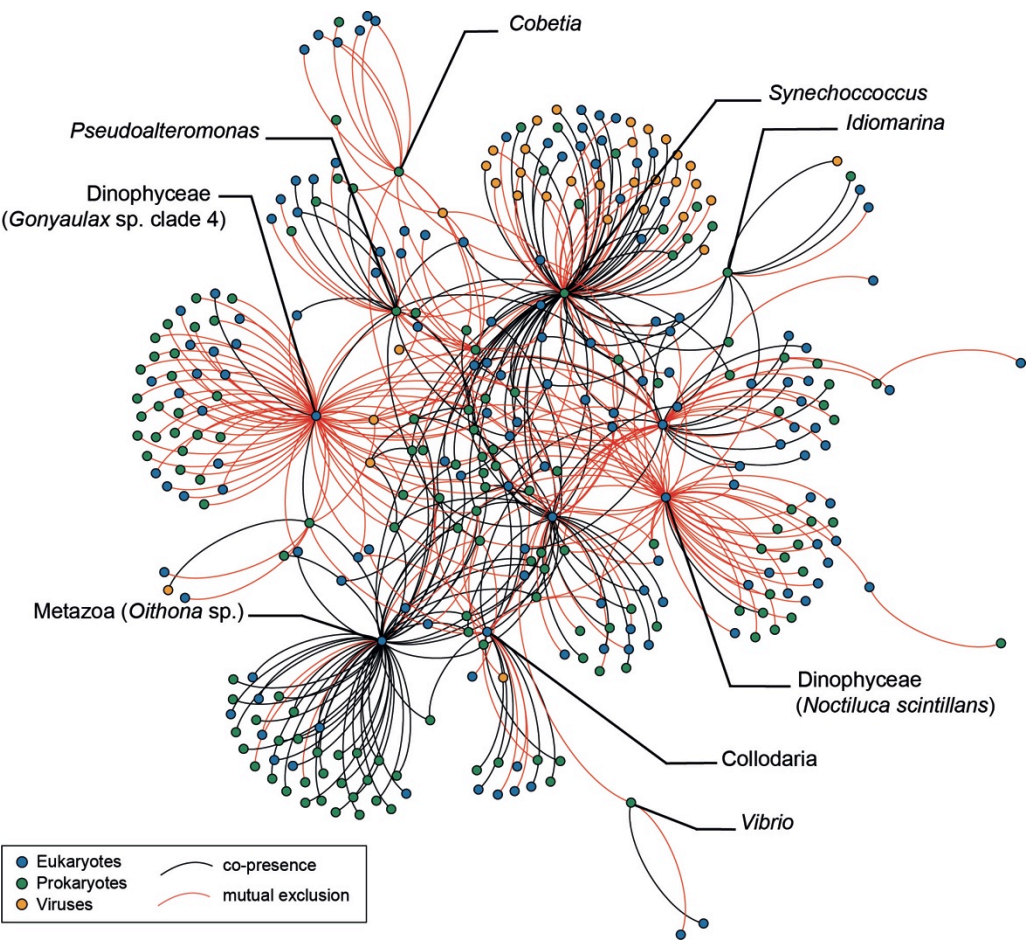891   Figure 1

892

893

Figure 2

894
895
896
897

898
899

Figure 3

900

901

902

903
904

Figure 4

905

906

907

908
909

a

1

Correlation to carbon export

⬤ **High VIP score functions:**
Unknown
Predicted membrane protein
Superfamily II DNA/RNA helicases, SNF2 family
Unknown
ABC-type sugar transport systems, permease components
Predicted membrane protein
Unknown
Protein involved in photosynthesis

0

Increasing VIP (PLS CV-R^2 = **0.41**)

1

Correlation to carbon export

⬤ **High VIP score functions:**
Transcriptional activator of acetoin/glycerol metabolism
Peroxiredoxin
ABC-type sugar transport systems, ATPase components
ABC-type sugar transport system, permease component
Protein involved in protein secretion
Uncharacterized conserved protein
Unknown
Predicted chitinase

0

Increasing VIP (PLS CV-R^2 = **0.48**)

b

77% unknown or general function   123 OGs VIP>1

58% unknown or general function   54 OGs VIP>1

0.0   0.2   0.4   0.6   0.8   1.0

☐ Function unknown
☐ General function prediction only
☐ Carbohydrate transport and metabolism
☐ Transcription
☐ Inorganic ion transport and metabolism
☐ Replication, recombination and repair
☐ Signal transduction mechanisms
☐ Energy production and conversion

☐ Post-translational modification, protein turnover
☐ Cell wall/membrane/envelope biogenesis
☐ Lipid transport and metabolism
☐ Translation, ribosomal structure and biogenesis
☐ Coenzyme transport and metabolism
☐ Secondary metabolites biosynthesis, transport
☐ Cell motility
☐ Nucleotide transport and metabolism

910

911   Figure 5

912

a) Pairwise approach

OTU

samples

Correlation of OTU with environnments

OTU

Correlation
-0.6 -0.3 0 0.3 0.6

p

b) Graph-based approach (WGCNA)

OTU

samples

Co-occurrence graph with scale-free topology

OTU

OTU

Clustering and subnetwork indentification

OTU

OTU

OTU

OTU

OTU

OTU

OTU

Relationship of the subnetwork topology and Carbon Export

p

$R^2>0.6$ p-value~0

OTU

Correlation to C. export

Subnetwork membership

c) Machine learning technique (PLS)

Correlation to C. export

R^2= x, p-value=y

Subnetwork membership

Reduction of OTU number while maintaining predictive power

R^2 ±x, p-value±y

OTU with high VIP

OTU with small VIP

Correlation to C. export

Subnetwork membership

913

914   Extended Data Figure 1

915

916

917

918

919   Extended Data Figure 2

920

921

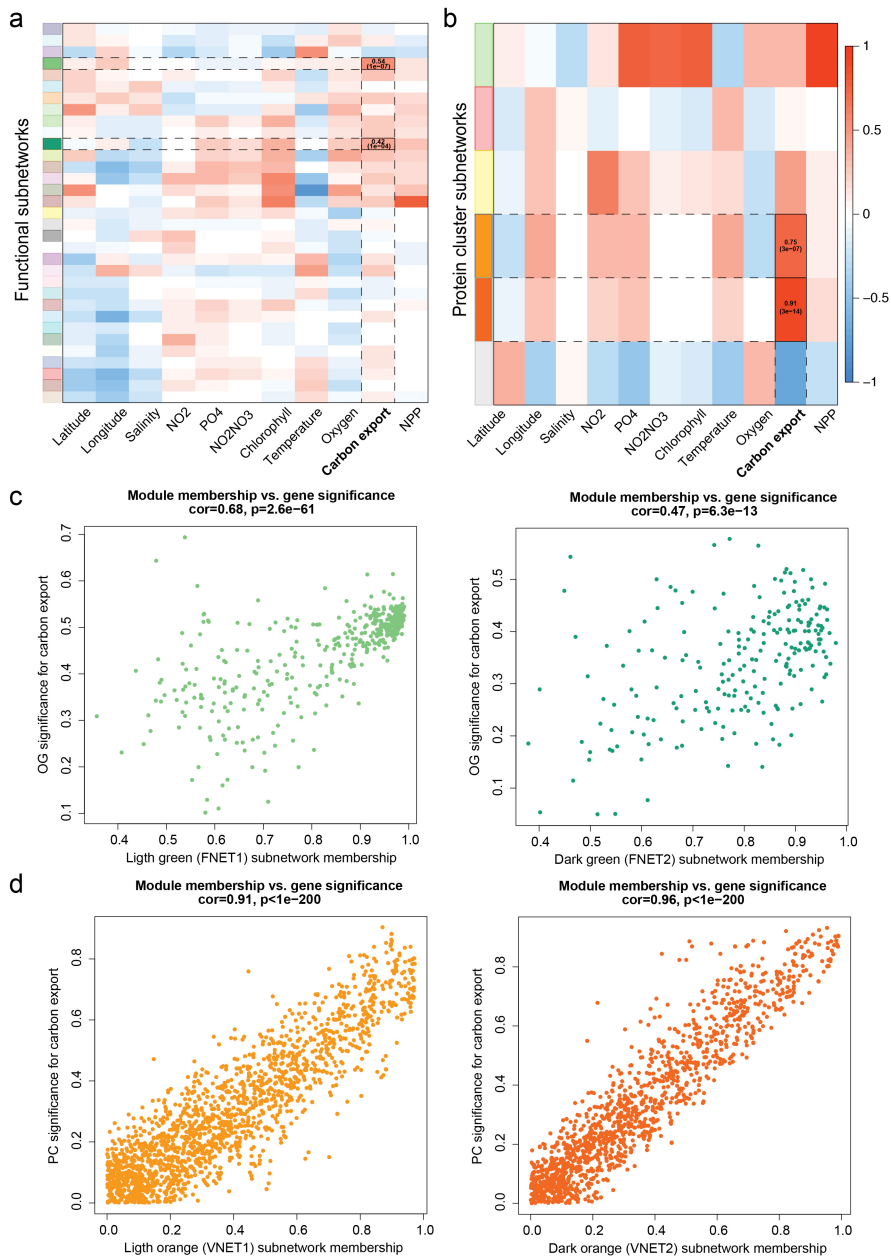922

923

924 Extended Data Figure 3

925

926
927
928

a

Proc. cell counts vs. Flux
cor = -0.13, p = 0.27

b

Syn. cell counts vs. Flux
cor = 0.64, p = 4.0^{e-10}

c

Syn. / Proc. cell counts ratio vs. Flux
cor = 0.54, p = 4.0^{e-07}

929

930   Extended Data Figure 4

931

932

933   Extended Data Figure 5

934
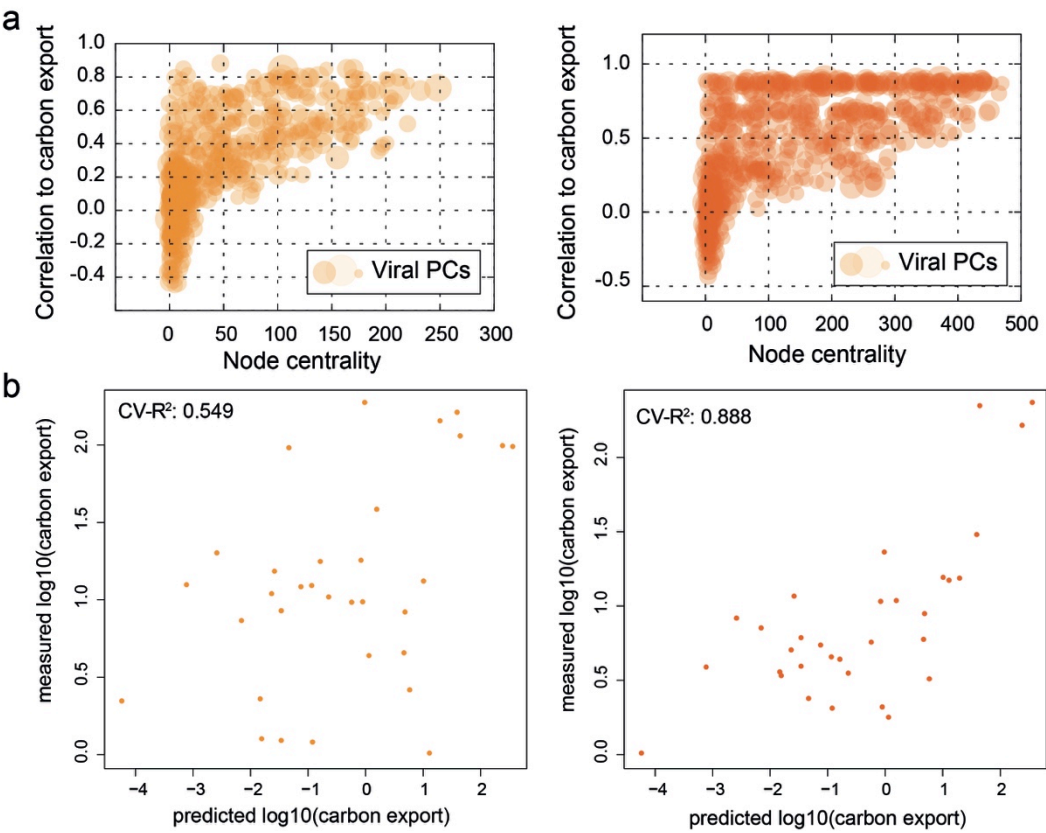
935

936

937

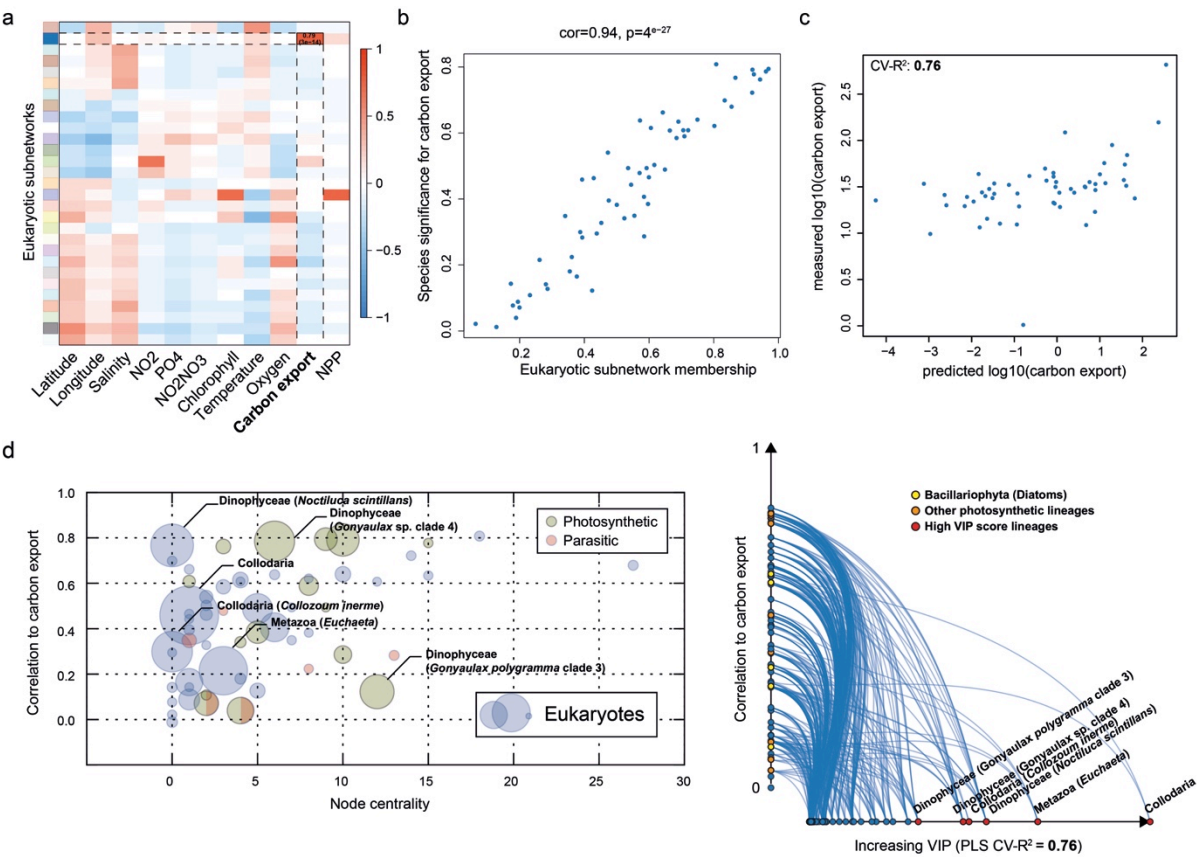938 Extended Data Figure 6

939

940
941

942

Extended Data Figure 7

943

944

945
946

947

948   Extended Data Figure 8